

Highlights

Extreme Precipitation Return Levels for Multiple Durations on a Global Scale

Gaby J. Gründemann, Enrio Zorzetto, Hylke E. Beck, Marc Schleiss, Nick van de Giesen, Marco Marani, Ruud J. van der Ent

- Global precipitation return levels for 3-hour to 10-day durations are analysed
- Three different extreme value distributions are used to estimate the extremes
- The MEV distribution shows the most coherent spatiotemporal patterns
- Two distributions show a global shift from heavy to thin tails for longer durations

Extreme Precipitation Return Levels for Multiple Durations on a Global Scale

Gaby J. Gründemann^{a,b}, Enrio Zorzetto^c, Hylke E. Beck^d, Marc Schleiss^e,
Nick van de Giesen^a, Marco Marani^f, Ruud J. van der Ent^{a,g,h}

^a*Department of Water Management, Faculty of Civil Engineering and Geosciences, Delft University of Technology, Delft, Netherlands*

^b*Centre for Hydrology, University of Saskatchewan, Canmore, Alberta, Canada*

^c*Program in Atmospheric and Oceanic Sciences, Princeton University, Princeton, New Jersey, USA*

^d*Department of Civil and Environmental Engineering, Princeton University, Princeton, New Jersey, USA*

^e*Department of Geoscience and Remote Sensing, Faculty of Civil Engineering and Geosciences, Delft University of Technology, Delft, Netherlands*

^f*Dipartimento di Ingegneria Civile, Edile ed Ambientale, Università degli Studi di Padova, Padova, Italy*

^g*Department of Physical Geography, Faculty of Geosciences, Utrecht University, Utrecht, Netherlands*

^h*Water Research Centre, School of Civil and Environmental Engineering, University of New South Wales, Sydney, Australia*

Abstract

Quantifying the magnitude and frequency of extreme precipitation events is key in translating climate observations to planning and engineering design. Past efforts have mostly focused on the estimation of daily extremes using gauge observations. Recent development of high-resolution global precipitation products, now allow estimation of global extremes. This research aims to quantitatively characterize the spatiotemporal behavior of precipitation extremes, by calculating extreme precipitation return levels for multiple durations on the global domain using the Multi-Source Weighted-Ensemble Precipitation (MSWEP) dataset. Both classical and novel extreme value distributions are used to provide an insight into the spatial patterns of precipitation extremes. Our results show that the traditional Generalized Extreme Value (GEV) distribution and Peak-Over-Threshold (POT) methods,

Email address: g.j.gruendemann@tudelft.nl (Gaby J. Gründemann)

which only use the largest events to estimate precipitation extremes, are not spatially coherent. The recently developed Metastatistical Extreme Value (MEV) distribution, that includes all precipitation events, leads to smoother spatial patterns of local extremes. While the GEV and POT methods predict a consistent shift from heavy to thin tails with increasing duration, the heaviness of the tail obtained with MEV was relatively unaffected by the precipitation duration. The generated extreme precipitation return levels and corresponding parameters are provided as the Global Precipitation Extremes (GPEX) dataset. These data can be useful for studying the underlying physical processes causing the spatiotemporal variations of the heaviness of extreme precipitation distributions.

Keywords: Precipitation extremes, MSWEP, Metastatistical extreme value distribution, Generalized extreme value distribution, Peaks-over-threshold, Global domain

PACS: 92.40.-t, 92.40.Ea, 92.70.Np, 02.50.-r

2000 MSC: 86A05

1 Introduction

Extreme precipitation events are a major contributor to natural disasters (CRED, 2019). Accurate estimates of the severity of intense precipitation events are needed for an enhanced disaster risk understanding, such as that of floods and landslides. The urgency of this is indicated as the first priority of the Sendai Framework for Disaster Risk Reduction (UNSIDR, 2015). The accurate quantification of extremes is also necessary for infrastructure planning and design. Some countries already provide spatiotemporal estimates of extreme precipitation based on extreme value distributions (EVDs), for example, for Australia (Ball et al., 2019), the Netherlands (Beersma et al., 2018), and the US (e.g., Perica et al., 2015, 2018). However, many countries and regions do not have sufficient local data available (Gründemann et al., 2018; Kidd et al., 2017; van de Giesen et al., 2014), such that spatially-distributed extreme precipitation estimates are not possible.

Several previous studies have developed global-scale datasets of extreme precipitation. Courty et al. (2019) calculated intensity-duration-frequency curves at the global domain and their scaling with different event durations using reanalysis data and the Generalized Extreme Value (GEV) distribution with fixed tail behavior. Donat et al. (2013) produced the HadEx-2

20 dataset, which contains 29 generic precipitation and temperature indices,
21 although these indices are not based on EVDs. Furthermore, this dataset
22 has a coarse 2.50° latitudinal \times 3.75° longitudinal resolution, with data-
23 gaps due to insufficient available gauge data. Other global studies mostly
24 focused on examining which type of distribution is most suitable to capture
25 the tail behavior of extreme precipitation (Cavanaugh and Gershunov, 2015;
26 Cavanaugh et al., 2015; Papalexiou et al., 2013). In addition, the spatial
27 patterns of the parameter controlling the tail decay have been studied for
28 the GEV distribution (Papalexiou and Koutsoyiannis, 2013; Ragulina and
29 Reitan, 2017), and the Generalized Pareto (GP) distribution (Serinaldi and
30 Kilsby, 2014). However, several issues remain to be addressed in order to
31 obtain global-domain extreme precipitation return levels: 1) the choice of
32 the dataset, 2) the focus on daily durations, 3) the choice of the time blocks
33 over which block-maxima are determined, and 4) the exploration of possi-
34 ble alternatives to the classical EVDs and the associated uncertainty with
35 respect to the tail behavior.

36 1. Several (quasi-)global gridded precipitation datasets have been devel-
37 oped in the recent years, each with strengths and weaknesses. See Sun
38 et al. (2018) and Beck et al. (2019a) for recent overviews of available
39 datasets. Most of these datasets are based on gauge, reanalysis, or
40 satellite sensor data. Notable examples of gauge-based datasets in-
41 clude GPCC-FDR (Becker et al., 2013; Schneider et al., 2011) and
42 REGEN (Contractor et al., 2020). However, gauges are extremely un-
43 evenly distributed across the globe (Kidd et al., 2017; Schneider et al.,
44 2014), and the number of active gauges has been declining in recent
45 decades (Mishra and Coulibaly, 2009). Satellite-based products such
46 as CMORPH (Joyce et al., 2004), GSMaP (Ushio et al., 2009), IMERG
47 (Huffman et al., 2015), and PERSIANN (Hong et al., 2004) have a rel-
48 atively high spatio-temporal resolution. However, they do not cover
49 regions outside of 60°N/S , and are only available from 2000 onwards,
50 which significantly hinders their use for extreme value analyses. Pre-
51 cipitation products with a true global coverage and long records are
52 reanalyses, such as ERA-5 (Hersbach et al., 2020), JRA-55 (Kobayashi
53 et al., 2015), and MERRA-2 (Gelaro et al., 2017). However, reanaly-
54 sis products tend to exhibit strong systematic biases in the magnitude
55 and frequency of precipitation (Decker et al., 2012; Liu et al., 2018;
56 Ménégoz et al., 2013).

- 57 2. Global-scale analyses of precipitation extremes are generally based on
58 daily precipitation records (Cavanaugh et al., 2015; Koutsoyiannis,
59 2004a,b; Papalexiou and Koutsoyiannis, 2013; Papalexiou et al., 2013;
60 Ragulina and Reitan, 2017; Serinaldi and Kilsby, 2014). In practice,
61 however, multiple durations are needed for the design of infrastruc-
62 ture (e.g., Nissen and Ulbrich, 2017) or urban drainage networks (e.g.,
63 Mailhot and Duchesne, 2009). It is known that precipitation extremes
64 of different durations scale differently with temperature (Wasko et al.,
65 2015), but little is known about the variation of EVD properties (tail
66 behavior) for different temporal resolutions. Studies that did derive
67 extreme precipitation statistics for durations ranging from minutes to
68 a few days have mostly focused on small regions (McGraw et al., 2019;
69 Nissen and Ulbrich, 2017; Overeem et al., 2008).
- 70 3. Studies estimating return levels of extreme precipitation by using an-
71 nual maxima typically use calendar years to delineate the annual pe-
72 riods from which maxima values are extracted (e.g., De Paola et al.,
73 2018; Marani and Zanetti, 2015; Papalexiou and Koutsoyiannis, 2013;
74 Ragulina and Reitan, 2017; Villarini et al., 2011). When the variable
75 of interest is river discharge instead of precipitation, however, hydro-
76 logical years are typically used instead of calendar years to determine
77 the annual maxima (Ward et al., 2016). For discharge values this is
78 important, since peak discharge and flooding could occur during 31
79 December to 1 January transition and one event would be included in
80 two calendar years. Although not often considered, this could also hap-
81 pen for precipitation. The annual maxima method could pick multiple
82 values from a single rainy season that may, for example, be highly influ-
83 enced by the El Niño-/Southern Oscillation, which is known to impact
84 precipitation extremes (Allan and Soden, 2008; Rasmusson and Arkin,
85 1993).
- 86 4. The Generalized Extreme Value (GEV) distribution, the most widely
87 used EVD, is typically fitted through one of two approaches: a) using
88 annual maximum precipitation series and maximum likelihood (Coles,
89 2001) or L-moment (Hosking, 1990) estimation approaches, or b) us-
90 ing a Peak-Over-Threshold (POT) method to fit a Generalized Pareto
91 Distribution to excesses above the threshold and a Poisson process to
92 the sequence of threshold exceedances (Coles, 2001). In contrast to
93 GEV and POT, the recently developed Metastatistical Extreme Value
94 (MEV) distribution is fitted using all events with recorded precipita-

95 tion instead of only the most severe. The inclusion of more events re-
96 duces the uncertainty due to sampling effects, which is important when
97 dealing with short time series (Hu et al., 2020; Marani and Ignaccolo,
98 2015; Marra et al., 2018, 2019a; Miniussi and Marani, 2020; Zorzetto
99 et al., 2016; Zorzetto and Marani, 2019). This is particularly advanta-
100 geous when analyzing short remote sensing precipitation products, as
101 the commonly applied GEV requires many years of data to accurately
102 estimate the tail of the distribution (Papalexiou and Koutsoyiannis,
103 2013). Additionally, GEV parameter estimation depends heavily on a
104 few large values, which makes it very sensitive to the possible presence
105 of outliers, a relatively common occurrence in remote sensing estimates
106 of precipitation amounts (Zorzetto and Marani, 2020). The GEV tail
107 behavior is mostly controlled by its shape parameter, which is very
108 sensitive to sampling effects and the choice of the method used for es-
109 timation. To overcome these problems, some studies have suggested
110 to use one universal value of the shape parameter that is applicable to
111 the whole world Koutsoyiannis (2004a,b), or a shape parameter value
112 within a narrow range between exponential and heavy-tail behavior
113 (Papalexiou and Koutsoyiannis, 2013), or one shape parameter per re-
114 gion, that is similar within climate types and elevation ranges (Ragulina
115 and Reitan, 2017). The estimation of the shape parameter is partic-
116 ularly difficult with short data series, though crucial for the accurate
117 estimation of extremes.

118 In this study we contribute to overcome these issues by 1) using a dataset
119 that merges all three main sources of precipitation data, 2) estimating ex-
120 tremes for several event durations, 3) using hydrological years in our analyses,
121 and 4) comparing results from three different extreme value methods (GEV,
122 POT and MEV). Specifically, we are interested in quantitatively character-
123 izing the behavior of extreme precipitation and the spatiotemporal variation
124 of extreme value distributional tails at the global domain.

125 2. Material and Methods

126 2.1. Data

127 The global precipitation product used in this study is the Multi-Source
128 Weighted-Ensemble Precipitation (MSWEP-V2.2) dataset. MSWEP is par-
129 ticularly suited for our purpose due to its global coverage, long temporal

130 span, high spatial and temporal resolution. We used data from 1 January
131 1979 to 31 October 2017 at a 0.1° latitude \times 0.1° longitude resolution at
132 3-hourly time steps. We selected all land-cells between 90°N and 58°S for
133 our analysis. MSWEP precipitation estimates are derived by merging five
134 different satellite- and reanalysis-based global precipitation datasets. The
135 dataset is one of the few precipitation products with daily (as opposed to
136 monthly) gauge corrections, applied using a scheme that accounts for gauge
137 reporting times (Beck et al., 2019b). MSWEP has shown robust performance
138 compared to other widely used precipitation datasets (e.g., Alijanian et al.,
139 2017; Bai and Liu, 2018; Beck et al., 2017, 2019a; Casson et al., 2018; Hu
140 et al., 2020; Sahlu et al., 2017; Satgé et al., 2019; Zhang et al., 2019), thus
141 underlying its potential for improving the characterization of extreme pre-
142 cipitation worldwide. We refer to Beck et al. (2019b) for a comprehensive
143 description of the dataset.

144 *2.1.1. Quality Control*

145 The integration of erroneous gauge observations into MSWEP-V2.2 can
146 occasionally result in implausible precipitation values. Therefore, we imple-
147 mented a three-step quality control procedure of the 3-hourly data prior to
148 the analysis. We first discarded negative values, which are physically impos-
149 sible. The second step was to discard outliers, which we defined as values
150 deviating from the mean by more than 30 standard deviations. We also dis-
151 carded data surrounding the outliers for the same time step using a 11×11
152 grid-cell window, as erroneous gauge observations may have influenced sur-
153 rounding cells in the production of the MSWEP dataset. The third step
154 was to discard years with > 30 missing days or < 5 ‘wet’ 3-hourly periods,
155 identified using a threshold of $0.2 \text{ mm } 3\text{h}^{-1}$ following Wasko et al. (2015).
156 Finally, we only included in the analysis data from grid cells with at least
157 30 years of data remaining, as a minimum record length of 30 years is cus-
158 tomary and recommended to obtain reliable results (Arguez and Vose, 2011;
159 Kendon et al., 2018; Westra et al., 2013).

160 *2.1.2. Durations and Identification of Independent Events*

161 The durations we selected for our analysis are 3, 6, 12 and 24 hours, and
162 2, 3, 5 and 10 days. In order to create statistically-independent precipitation
163 events for multiple durations, we first separated 3-hourly events following the
164 declustering method to limit the autocorrelation of the samples described in
165 Marra et al. (2018, their Section 3.1). For longer durations, independent

166 events are the maximum intensities within each independent event and non-
167 overlapping period using moving windows (Marra et al., 2020).

168 *2.1.3. Hydrological Year*

169 A common challenge in global-scale assessments is the delineation of the
170 hydrological year, given the regional variability in the climatological precip-
171 itation seasonality. We therefore developed an uniform way to define the
172 hydrological year. To avoid splitting one rainy season over two different
173 years, we computed the median of the monthly precipitation for each grid-
174 cell, and defined the start of the hydrological year to be the first day of the
175 driest month. Supplementary Material Figure S1a shows the starting month
176 of the hydrological year as determined by this method. These data are also
177 available in the GPEX dataset (Gründemann et al., 2021). As MSWEP-V2.2
178 spans the interval from 1 January 1979 to 31 October 2017, we discarded the
179 data prior to the start of the first hydrological year, thus keeping 38 complete
180 years. Only where the hydrological year starts in December there are just 37
181 complete years, which occurs in 5.8% of the grid cells.

182 We also investigated whether there is a significant difference between the
183 use of calendar and hydrological years for the estimated daily extremes for
184 GEV and MEV. The POT method is based on the values over a high thresh-
185 old, irrespective of when they occurred. Therefore, there is by definition no
186 difference in calculating the extremes using hydrological or calendar years
187 for the POT method. To determine the difference for GEV and MEV, we
188 first calculated the daily return levels for normal calendar years, using the
189 MSWEP data from 1979 to 2016. Second, we calculated the return levels for
190 the same distributions and the same years, by removing the months before
191 the start of the hydrological year from the year 1979 and adding them to the
192 year 2016. We did this in order to use the exact same data, so the differences
193 in the return level estimates are solely due to a different starting month.

194 *2.2. Extreme Value Distributions*

195 Three extreme value distributions were fitted to the MSWEP data to
196 calculate extreme precipitation return levels: the GEV, POT, and MEV
197 distributions. Annual (hydrological year) maxima were used to estimate the
198 three parameters of the GEV using the L-moments approach, because of its
199 robust performance for small samples (Hosking, 1990). The GEV cumulative

200 distribution function (CDF) is given by:

$$G(z) = \begin{cases} \exp \left\{ - \left[1 + \xi \left(\frac{z-\mu}{\sigma} \right) \right]^{-\frac{1}{\xi}} \right\}, \xi \neq 0 \\ \exp \left\{ -\exp \left[- \left(\frac{z-\mu}{\sigma} \right) \right] \right\}, \xi = 0 \end{cases} \quad (1)$$

201 with location parameter $\mu \in (-\infty, \infty)$, scale parameter $\sigma > 0$, and shape
 202 parameter $\xi \in (-\infty, \infty)$. The annual extremes estimated by GEV are trans-
 203 lated into those of the parent distribution, following Koutsoyiannis (2004a,
 204 equation 3).

205 As a second EV model we use a Peaks Over Threshold approach, de-
 206 scribing precipitation accumulations exceeding a high threshold using a GP
 207 distribution, while modelling the frequency of threshold exceedances using a
 208 Poisson point process (Coles, 2001; Davison and Smith, 1990). This frame-
 209 work also yields GEV as the resulting extreme value distribution, which is
 210 then used to determine the quantile corresponding to a given return period.
 211 The GP CDF is given by:

$$H(y) = \begin{cases} 1 - \left(1 + \frac{\xi y}{\beta} \right)^{-\frac{1}{\xi}}, \xi \neq 0 \\ 1 - \exp \left(-\frac{y}{\beta} \right), \xi = 0 \end{cases} \quad (2)$$

212 where $y > 0$ are precipitation excesses over the threshold, with $\beta > 0$ and
 213 $\xi \in (-\infty, \infty)$ the GP scale and shape parameters respectively. A relevant
 214 aspect in applying the POT model is a suitable choice of the threshold used
 215 to define precipitation exceedances. Our global-scale application requires
 216 studying the distribution of precipitation extremes across markedly different
 217 climatic regions, thus excluding the adoption of a constant threshold value.
 218 We studied the effect of the threshold choice using multiple threshold selec-
 219 tion methods on a global sample of grid cells (see Supplementary Material
 220 Section 2 and and Figure S2). Our results showed that this choice had a lim-
 221 ited effect on the estimated return levels (Figure S2a). We chose to perform
 222 our global analysis by selecting for each cell a threshold value such that it
 223 is exceeded on average 3 times each hydrological year. As a consequence of
 224 this choice, the sample size available for fitting the GP distribution remains
 225 constant across different precipitation durations. The method used to fit
 226 the GP distributions is the Probability Weighted Moments (PWM; e.g., see
 227 Hosking and Wallis, 1987).

228 The third model applied here is the MEV distribution (Hosseini et al.,
 229 2020; Hu et al., 2020; Marani and Ignaccolo, 2015; Miniussi et al., 2020a,b;

230 Zorzetto et al., 2016). In the MEV framework, all “ordinary” precipitation
 231 events, i.e. all events above a small threshold, are used to infer this EV
 232 distribution. The threshold we applied is $0.2 \text{ mm } 3\text{h}^{-1}$, coinciding with
 233 the earlier defined ‘wet event’. Weibull parameters were estimated for each
 234 hydrological year separately, based on all wet events using the PWM method
 235 (Greenwood et al., 1979) as done in Zorzetto et al. (2016). The MEV-Weibull
 236 CDF is given by:

$$\zeta_m(x) = \frac{1}{M} \sum_{j=1}^M \left\{ 1 - \exp \left[- \left(\frac{x}{C_j} \right)^{w_j} \right] \right\}^{n_j} \quad (3)$$

237 where j is the hydrological year ($j = 1, 2, \dots, M$), $C_j > 0$ is the Weibull scale
 238 parameter, $w_j > 0$ is the Weibull shape parameter, and n_j is the number of
 239 wet events observed in hydrological year j (Marani and Ignaccolo, 2015).

240 2.2.1. Observed Return Period

241 The MSWEP dataset analyzed here has 38 complete years of data. There-
 242 fore, the empirical return period associated with the maximum value on
 243 record computed according to the Weibull empirical frequency estimate is
 244 $T_{\text{observed}} = 39$ years. However, only 91% of all cells had 38 complete years
 245 of data, so the maximum observed return period is sometimes lower: for 7%
 246 of the cells only 37 complete years were available, and for 2% of the cells
 247 36 years or less were available. However, for simplicity we still refer to the
 248 corresponding maximum return level as T39 in the results.

249 2.2.2. Tail Behavior

250 Both the GEV and MEV distributions are flexible and can describe dif-
 251 ferent tail behaviors. They are, therefore, appropriate models to study the
 252 characteristics of local precipitation extremes. The tail behavior of the two
 253 distributions differs, as illustrated in Figure S3 for different combinations of
 254 scale and shape parameters. The shape parameter ξ of the GEV distribution,
 255 obtained either through the annual maxima or POT approach, encodes the
 256 nature of the tail of the distribution. Based on the value of ξ , the GEV can
 257 take one of three forms: a positive GEV shape parameter ($\xi > 0$, “Fréchet”)
 258 corresponds to a power-law tail, i.e., to a slowly-decaying probability of large
 259 events. This heavy-tail behavior contrasts with the case of an exponential
 260 tail ($\xi = 0$, “Gumbel”), and with the case of a distribution with an upper end

261 point, which corresponds to negative values of the shape parameter ($\xi < 0$,
 262 “inverse Weibull”).

263 The MEV distribution assumes that precipitation events are Weibull-
 264 distributed. The tail decay of this distribution is controlled by its shape
 265 parameter: for $w < 1$ its tail behavior is “sub-exponential”, i.e., heavier than
 266 that of an exponential (recovered for $w = 1$), albeit with a characteristic
 267 scale (Laherrere and Sornette, 1998; Wilson and Toumi, 2005). For $w > 1$
 268 the Weibull tail is super-exponential, with a fast decaying tail, while still
 269 retaining an infinite upper end point. Hence, the shape parameter of the
 270 Weibull distribution encodes the propensity of a site to be subjected to large
 271 extreme events (Wilson and Toumi, 2005; Zorzetto et al., 2016). However,
 272 the tail decay of the MEV distribution is not only dependent on that of
 273 ordinary values (through w) but is also affected by the yearly number of
 274 events (Marra et al., 2018) and by the inter-annual variations of C_j, w_j, n_j .

275 In an effort to compare the heaviness between the distributions, we have
 276 come up with a measure of heaviness that is based on the return levels them-
 277 selves (Figure 1). The difference between the 1000-year return level and the
 278 10-year return level can be described as follows:

$$T1000 = T10 + b + b + a \tag{4}$$

279 Where b is the difference between the 100-year and 10-year return level,
 280 i.e.: $b = T100 - T10$, and a is the additional increase caused by the heaviness
 281 of the tail (Figure 1). A positive a is indicative of heavy tails and a negative
 282 a of thin tails. For pure exponential tails it holds that $a = 0$. The value for
 283 a is highly dependent on the local precipitation systems, so we defined the
 284 heaviness amplification factor h to be a normalization of a :

$$h = \frac{a}{b} = \frac{T1000 - 2 \times T100 + T10}{T100 - T10} \tag{5}$$

285 In words, the meaning of h is the fractional additional increase between
 286 T1000 and T100 that is more than the increase that could be expected from
 287 a pure exponentially tailed distribution. A distribution has a heavy tail for
 288 $h > 0$ and a thin tail for $h < 0$.

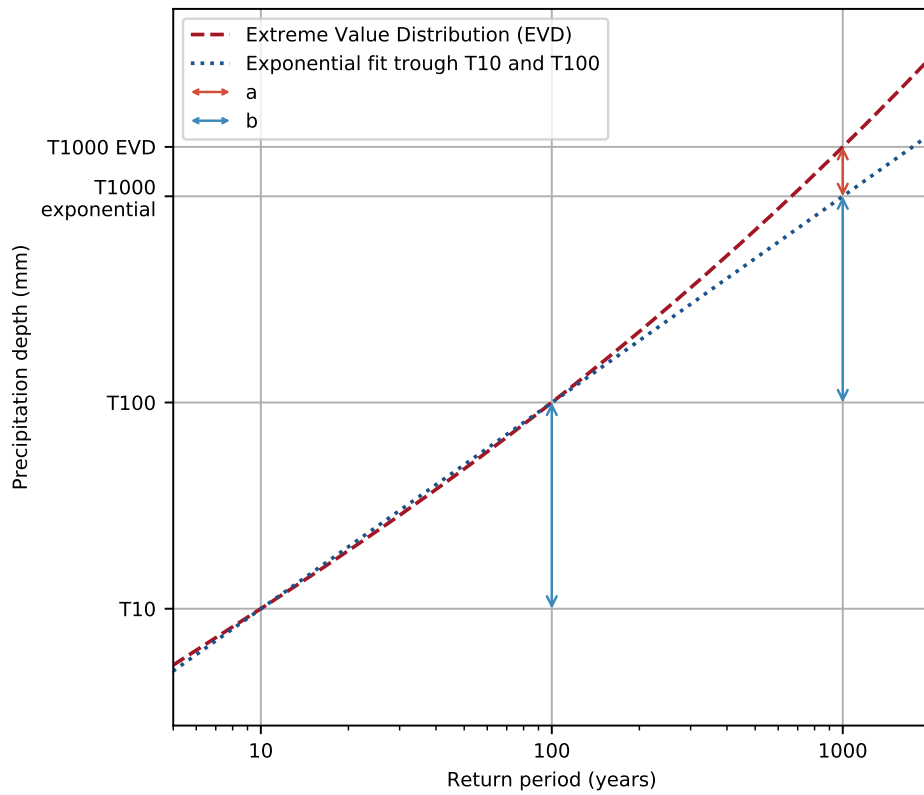


Figure 1: Illustration of our method to measure the tail heaviness for any distribution based on return levels only.

289 3. Results and Discussion

290 3.1. Hydrological Year

291 Figure 2 shows the frequency distribution of 1000-year return levels esti-
292 mated using calendar and hydrological years for GEV and MEV. The spatial
293 distribution of these differences is presented in Supplementary Material Fig-
294 ure S1b for GEV and Figure S1c for MEV. We found that in the case of GEV
295 quantiles, the fraction of sites characterized by differences within $\pm 0.5\%$ is
296 larger than that observed for MEV. When the hydrological year starts in the
297 winter months, the hydrological year is only shifted by a few months. In
298 such instances, the annual maxima mostly stay the same between the cal-
299 endar and hydrological years, though the included events could differ. For
300 GEV this means that for many cells there is almost no difference in the T1000
301 estimates, whereas for MEV the difference is small.

302 On the other hand, when the offset with a calendar year is approximately
303 6 months, around June, there are many different events included in the hy-
304 drological years compared to the calendar years. This results in different
305 annual maxima and large differences in the estimated extremes for GEV
306 and MEV. The differences are most pronounced in the Southern hemisphere
307 and in locations where the hydrological year starts around June, e.g., in
308 the Mediterranean region, in the Middle-East, in Southern Africa, in Brazil,
309 around Indonesia, and in the western US (Figure S1a). For MEV the overall
310 sensitivity remains lower than that of GEV. In particular, the distribution
311 of differences in Figure 2 exhibits thicker tails for GEV (e.g., as measured
312 by the wider 5th to 95th percentile interval). This suggests that regional
313 sensitivity to the definition of block maxima can be quite significant for the
314 GEV approach.

315 3.2. Extreme Precipitation Estimates

316 Figure 3 shows the 100-year precipitation return levels for a 24-hour dura-
317 tion. Extreme value estimates for other durations and return periods are fea-
318 tured in the Global Precipitation EXtremes (GPEX) dataset (Gründemann
319 et al., 2021). The spatial patterns of the extremes estimated by GEV and
320 MEV are similar to Zorzetto and Marani (2020, their Figure 9), while the
321 spatial pattern of the underlying GEV parameters are consistent with Courty
322 et al. (2019, their Figure 1). The global spatial pattern of return levels for the
323 three EV methods is similar, although large regional differences can be ob-
324 served. The GEV and POT results are similar in magnitude and show similar

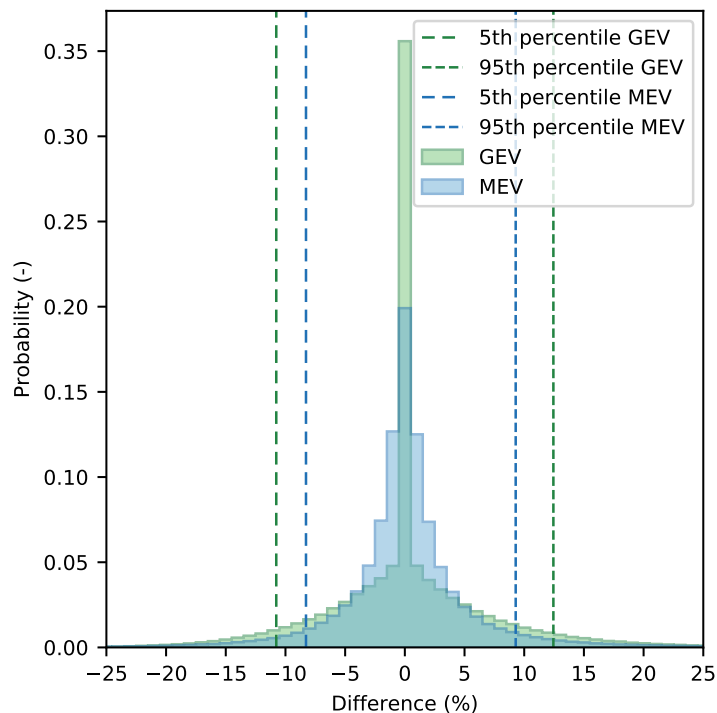


Figure 2: Weighted histogram showing the percentage difference in the values of T1000 quantiles calculated using calendar years and hydrological years. Included in the figure are all cells where the start of the hydrological year is different than the calendar year (i.e., the hydrological year does not start in January, see Supplementary Material Figure 1a). A negative difference indicates that the T1000 estimate is larger using hydrological years, whereas a positive difference indicates that the T1000 estimate is larger using calendar years.

325 differences when compared to MEV. The estimated precipitation extremes
 326 are generally lower for both GEV and POT compared to MEV quantiles.
 327 MEV estimates exhibit smooth spatial patterns, whereas the spatial pat-
 328 terns using GEV and POT are more irregular, consistent with the results of
 329 Zorzetto and Marani (2020) for the conterminous US. The reduced spatial
 330 coherence in patterns of extremes for GEV and POT is particularly evident in
 331 the Great Plains of North America, and in Northern Russia, Southeast Asia,
 332 and Central Africa. Furthermore, our analysis (Figure 3) reveals the pres-
 333 ence of a large number of circular areas with heavier extremes, corresponding
 334 to the location of gauges used for correcting precipitation estimates in the

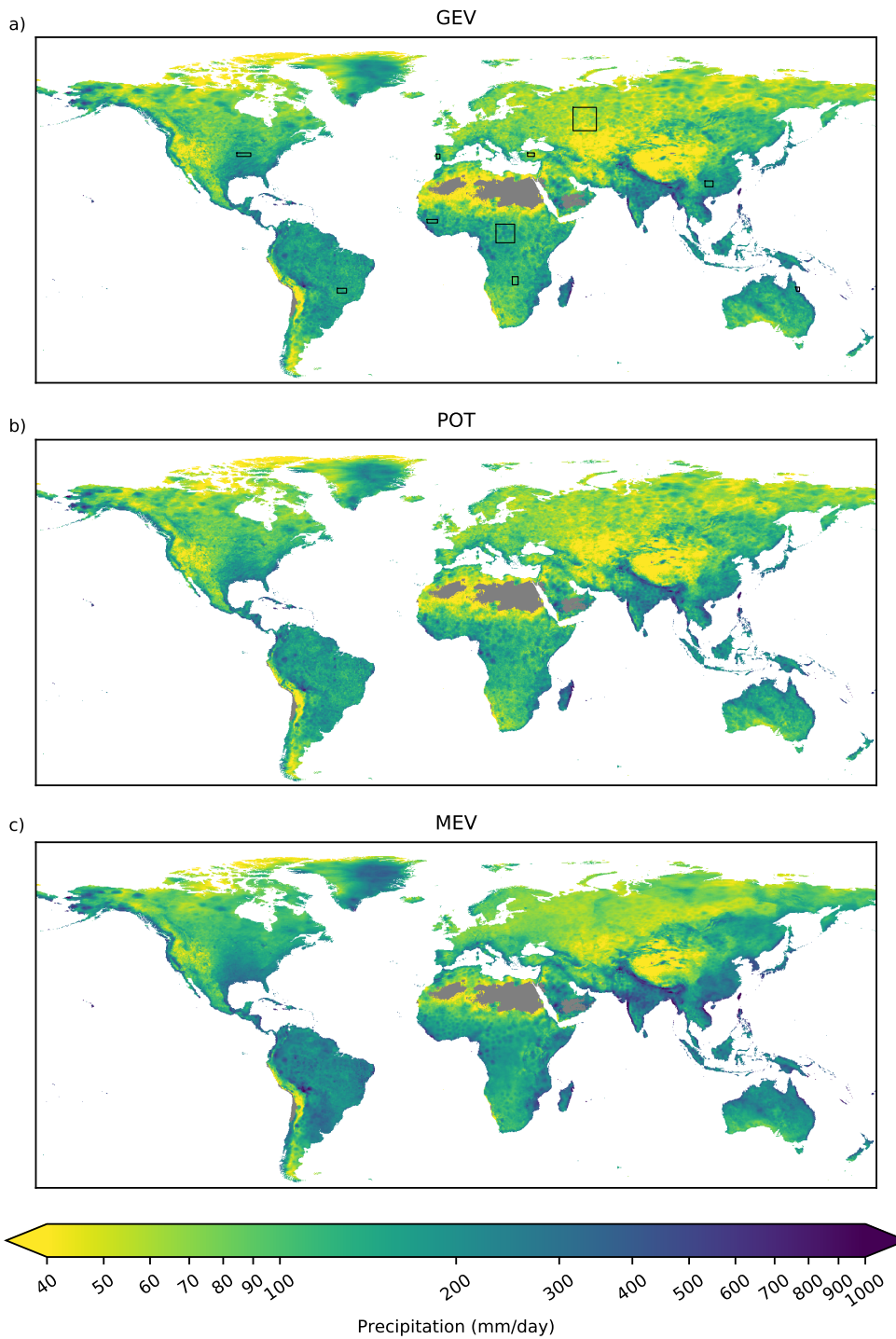


Figure 3: Precipitation return levels with a duration of 24-hours for a 100-year return period for different extreme value distributions: (a) the Generalized Extreme Value (GEV) distribution, (b) the Peak Over Threshold (POT) method, and (c) the Metastatistical Extreme Value (MEV) distribution. The black rectangles in panel a are the case studies corresponding to the areas in Figure 4.

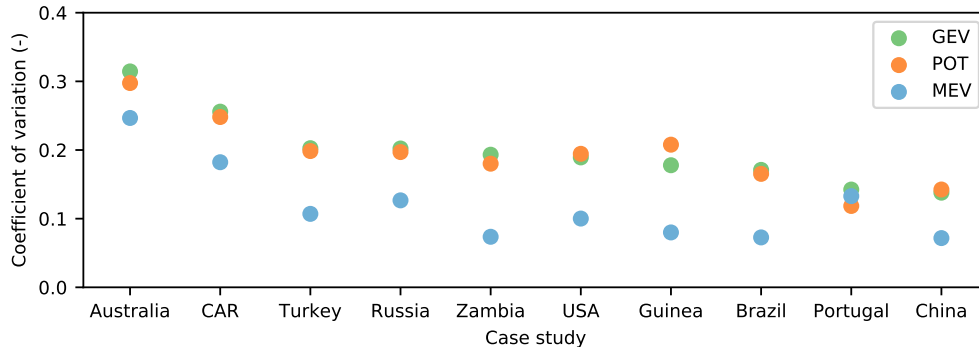


Figure 4: Coefficient of variation for the difference in estimated T100 quantiles for the three extreme value methods for 24-hour precipitation at selected case study areas. The coefficient of variation is the standard deviation of the precipitation divided by the mean precipitation. The locations of the case study areas are displayed in Fig 3a.

335 MSWEP algorithm (Beck et al., 2019b). The effect of these local correc-
 336 tions is much larger for traditional EV models (POT and GEV), while MEV
 337 appears less sensitive to these local corrections.

338 In order to study the ability of the three distributions to capture the
 339 spatial coherence of precipitation extremes, we selected several case study
 340 areas. They collectively cover a wide range of climates and domain sizes, the
 341 locations of which can be found in Figure 3a. Within a single case study
 342 area, we expect the precipitation estimates to be statistically homogeneous
 343 because of their precipitation generating mechanisms (Cavanaugh and Ger-
 344 shunov, 2015; Cavanaugh et al., 2015) or elevation (Ragulina and Reitan,
 345 2017). Figure 4a shows the coefficient of variation (CV) of T100 extreme
 346 precipitation estimates for these case studies. The CV is the ratio of the
 347 standard deviation to the mean and is used to compare the relative variation
 348 between the study areas. The higher the CV, the higher the relative spread
 349 of the precipitation estimates within a spatial domain. This figure shows
 350 quite similar behavior for GEV and POT, though POT has a slightly lower
 351 spread. The CV for MEV is lower, which points to more spatially coherent
 352 T100 precipitation estimates based on single point time series (with 38 years
 353 of training data).

354 To further investigate the global differences in magnitude between the
 355 three methods, we examine the extremes for each distribution using a spa-
 356 tially weighted mean over the global land surface. This is displayed for

357 multiple return periods and durations as depth-duration-frequency curves
358 (Figure 5). We first compare the maximum precipitation observed in the
359 dataset to the precipitation predicted from each distribution. As there are
360 38 complete years of MSWEP data, the maximum empirically observed re-
361 turn level is 39 years (T39 observed, the black dotted line in Figure 5). While
362 locally the empirical T39 estimate could be very different from the true re-
363 turn level, we expect the global average of this value to be representative
364 of the true T39. For GEV and POT, we expected the estimated T39 to be
365 close to the observed value since only the largest values are used to fit these
366 distributions. For MEV, we did not necessarily expect a good agreement for
367 T39, but its performance should be better for return levels greater than the
368 length of the observation time series (Marra et al., 2018, 2019b; Schellander
369 et al., 2019; Zorzetto et al., 2016). The results in Figure 5 show that for
370 the lower duration events, the observed T39 is close to the T39 for all three
371 distributions. For increasing durations, the deviation between empirically
372 observed and EV modeled T39 quantiles increases, particularly for MEV.
373 Both GEV and POT show an underestimation and MEV an overestimation.
374 This figure also shows again that the differences between GEV and POT are
375 small. The global average estimated extremes for GEV and POT are notably
376 lower than for MEV, as was already visible from Figure 3. This difference is
377 more pronounced for larger return periods and longer durations.

378 One reason the quantiles estimated using MEV are higher than using
379 GEV and POT is related to the increase in estimation uncertainty of Weibull
380 parameters when the number of events per hydrological year is low. This is
381 especially relevant in arid regions and for long durations. For instance, for 5
382 and 10-day durations the average annual number of events is 36 and 21 events
383 respectively. It is therefore possible that this leads to an overestimation by
384 MEV. To overcome this, windows of two or more years could result in a
385 better parameter estimation (Miniussi and Marani, 2020). A second factor
386 which may be relevant relevant for MEV quantile estimates is the use of a
387 fixed threshold for defining a precipitation event.

388 *3.3. Tail Behavior*

389 To better understand the differences between extremes estimated using
390 the three extreme value methods, we analyze their tail behavior using the
391 heaviness amplification factor h (Eq. 5). Figure 6 presents h for a 24-hour
392 duration worldwide for each of the three distributions. We refer to Figures S5-
393 S11 in Section 4 in the supplementary material for maps of h for the other

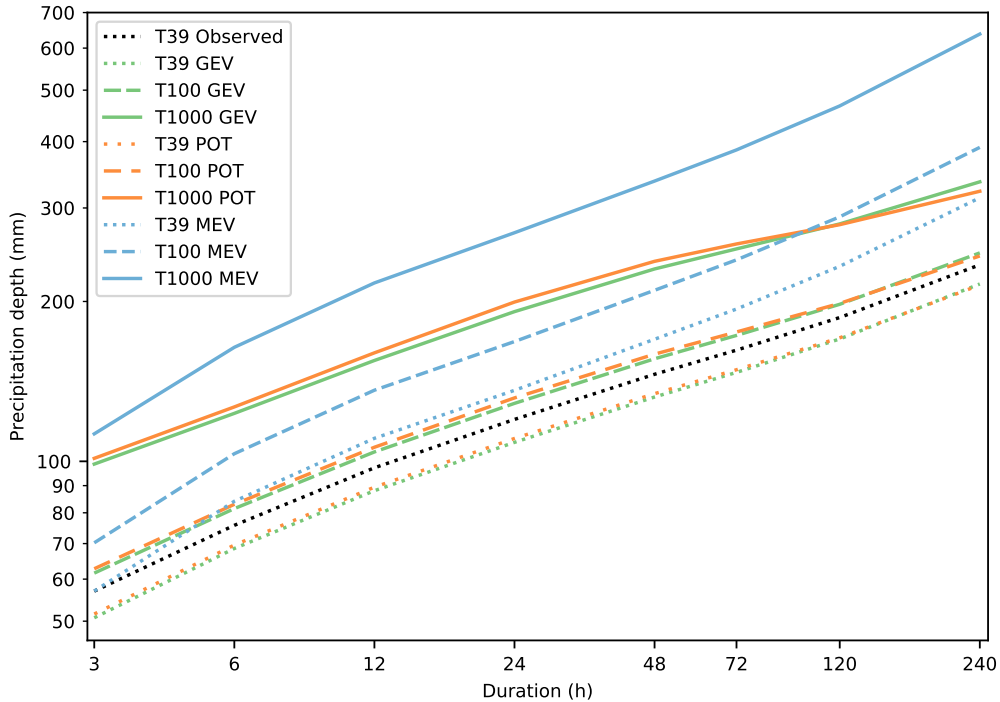


Figure 5: Area-weighted average depth-duration-frequency curves for the global land surface. T39 Observed is the mean spatially weighted maximum precipitation observed in the MSWEP-V2.2 dataset.

394 durations. Both GEV (Figure 6a) and POT (Figure 6b) exhibit a large
 395 spatial variability in addition to a low spatial coherence. This makes it
 396 difficult to discern clear spatial patterns with the exception of a few notable
 397 regions. For instance, in the Amazon, h is mostly negative, suggesting a
 398 tail with an upper limit, while in Eastern and Southern Australia h it is
 399 strongly positive, denoting strong heavy tail behavior. This map roughly
 400 corresponds to the spatial patterns of the daily GEV shape parameter shown
 401 by Papalexioiu and Koutsoyiannis (2013, their Figure 13) and Ragulina and
 402 Reitan (2017, their Figure 4). We also find that for the GEV and POT
 403 methods, grid cells associated with heavy tails can be adjacent to cells with
 404 thin tails. Furthermore, GEV and POT do not always show the same type
 405 of tail, heavy or thin, in the same grid cells. In 72% of the cases the sign of
 406 the underlying shape parameter agrees, while in 28% of the cases the signs
 407 are different for daily precipitation. This highlights the large uncertainty

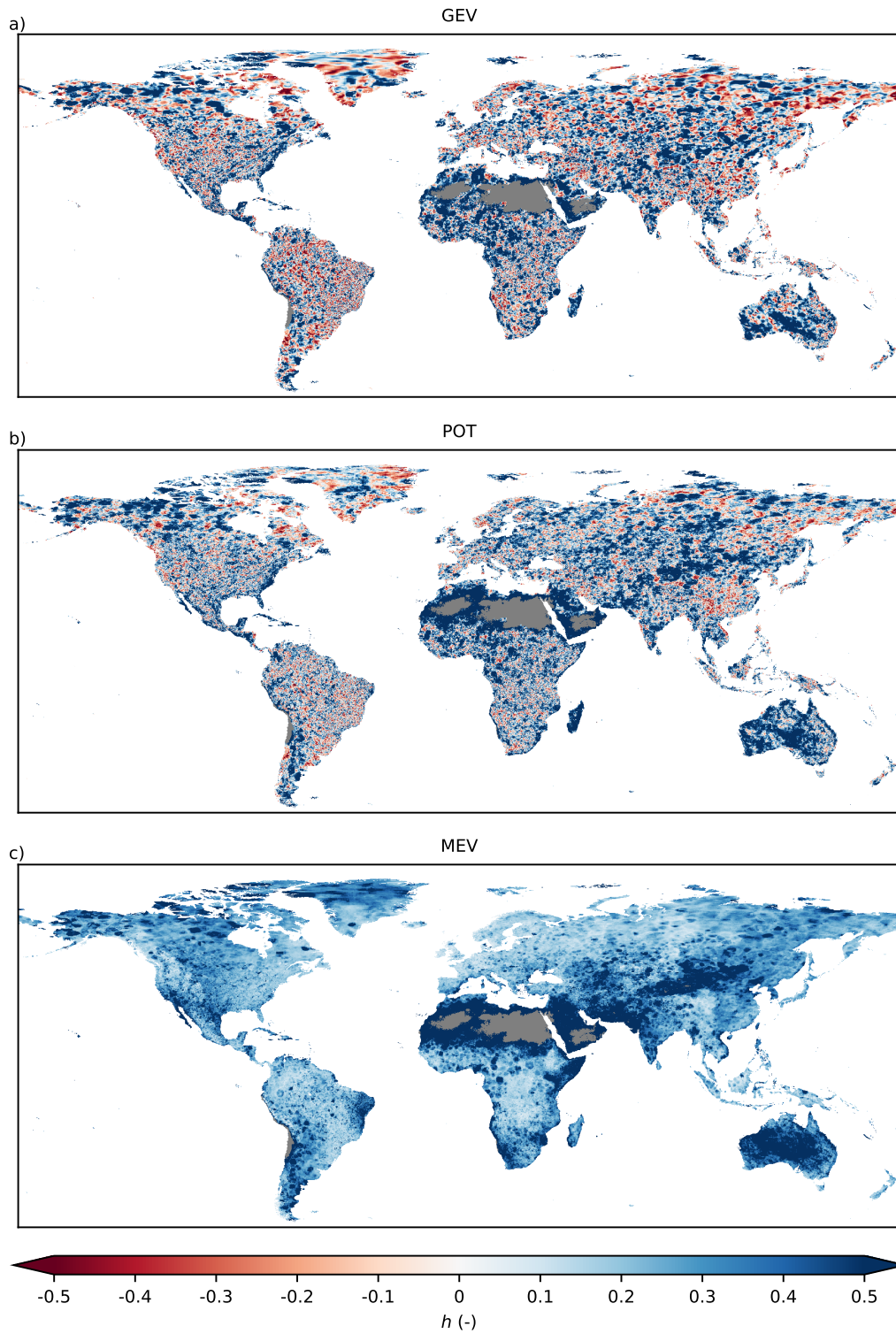


Figure 6: The heaviness amplification factor h (Eq. 5) for daily precipitation calculated for different extreme value methods: (a) GEV, (b) POT, (c) MEV. Red indicates a thin tail, white an exponential tail, and blue a heavy tail. See section 2.2.2 for more information on the heaviness metric, and Figures S5-S11 for maps of h for the other durations.

408 associated with estimating reliable tail parameters from short time series
409 and the sensitivity of the GEV and POT methods to sampling effects.

410 The heaviness of the MEV distribution (Figure 6c) shows a more coherent
411 spatial pattern. At virtually all grid cells the heaviness amplification factor
412 h (Eq. 5) indicates heavy tail behavior and there is a high consistency within
413 geographic regions and for all durations (Figures S5-S11). Based on previous
414 studies (Cavanaugh et al., 2015; Papalexiou and Koutsoyiannis, 2013; Pa-
415 papalexiou et al., 2013; Ragulina and Reitan, 2017), this predominantly heavy-
416 tail behavior of daily precipitation was expected and is well captured by
417 MEV. There are also topographical patterns visible in the heaviness amplifi-
418 cation factor (Figure 6c), though they are not as clearly distinguishable as for
419 the shape parameter itself (Figure S4). The heaviness tends to be higher in
420 arid areas, and lower in mountainous areas. Examples of arid areas with high
421 heaviness include the Sahara, the Namib and Kalahari in Africa, the Gobi,
422 Thar and Taklamakan in Asia, the Atacama Desert in South America, large
423 areas of Southwestern Australia, and the Arabian desert and other areas in
424 the Middle East. This same pattern is to a lesser extent also visible for the
425 heaviness of GEV (Figure 6a) and POT (Figure 6b).

426 At high elevations a small h is usually found for MEV (Figure 6c). Exam-
427 ples include the Rocky Mountains and the Sierra Madres in North America,
428 the northern Andes and large areas of the Brazilian Highlands in South Amer-
429 ica, the Ethiopian Highlands, the Scandinavian Mountains, and the Tibetan
430 Plateau. These spatial patterns are in contrast with what Papalexiou et al.
431 (2018, their Figure 6) found for hourly Weibull tails in the USA, where the
432 heaviest tails are in the mountainous areas, and the thin tails are in the
433 south-east. However, our results correspond well to Ragulina and Reitan
434 (2017, their Figure 4), who showed that heaviness decreases with elevation.

435 A comparison of the heaviness for different distributions and durations
436 is presented as a boxplot in Figure 7. For spatial maps of the heaviness
437 for the different durations we refer to Figures S5-S11. For GEV and POT,
438 predominantly heavy tails are observed for short durations and thinner tails
439 for long durations. Furthermore, GEV and POT both show a decreasing
440 variability in the heaviness for longer durations, indicated by both shorter
441 whiskers and boxes. The decrease of the heaviness of the tails for increasing
442 durations is in line with the findings of Cavanaugh and Gershunov (2015),
443 who found that longer duration extremes exhibit thinner tails. For GEV
444 and POT the longer durations largely indicate tails with a finite upper end
445 point. This occurs for instance in half of the cases for a duration of 10

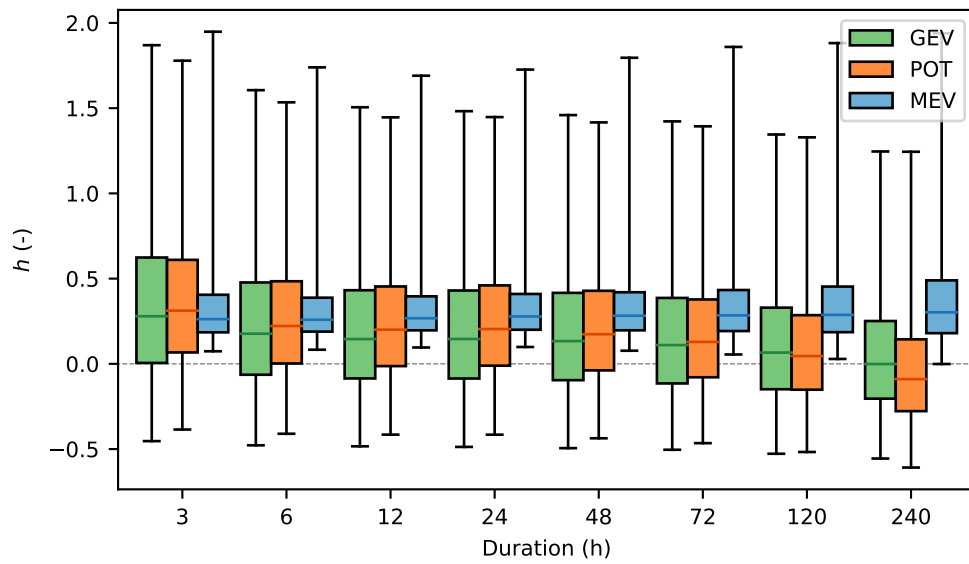


Figure 7: Boxplots showing the distribution of the heaviness amplification factor $h (-)$ for different durations and extreme value methods: (a) GEV and POT, and (b) MEV. The whiskers denote the 1st and 99th percentiles. The top and bottom of the boxes represent the 75th and 25th percentiles, respectively. The dashed gray horizontal lines indicate exponential tails. See section 2.2.2 for more information on the heaviness metric.

446 days for GEV, and more than half for POT. One implication of this finding
447 is that, when computing return levels for a single location (see Figures S3
448 and S12), it is possible for the very large return periods that the shorter
449 duration quantiles are more intense than the longer duration quantiles. This
450 is physically impossible (see Figure S12a,b,e and f), and we should thus be
451 extremely careful when interpreting such results.

452 MEV, on the other hand, shows different heaviness patterns than GEV
453 and POT (Figure 7 and Figures S5-S11). MEV shows almost entirely a
454 heavy-tail behavior, which remains consistent across the range of durations
455 examined. Furthermore, also the variability for MEV is constant across du-
456 rations, though with a slight increase for longer durations. The MEV distri-
457 bution thus produces a spatially and temporally coherent heavy tail behavior
458 based on a 38 years calibration sample and a single grid-cell analysis. This
459 is a promising result, as MEV, in contrast to the traditional methods ana-
460 lyzed, provides essential information on the spatial coherence of precipitation
461 extremes without any prior hypothesis on its spatial structure, for example
462 through a spatial clustering scheme (Demirdjian et al., 2018). In fact, the
463 spatial structure of the tail heaviness obtained through the MEV analysis
464 could be used as a measure of statistical homogeneity for regionalization
465 studies.

466 4. Conclusions

467 The aim of this research was to quantitatively characterize the spatiotem-
468 poral variation of global precipitation extremes and their associated extreme
469 value distribution tails. We have fitted three different extreme value methods
470 (GEV, POT, and MEV) to a global precipitation dataset, MSWEP V2.2, to
471 estimate extreme precipitation return levels for several durations. In order
472 to compare the tails of the three distributions, we introduced the heaviness
473 amplification factor h (Eq. 5). Instead of using calendar years to delineate
474 between different years, we used hydrological years. We demonstrated that
475 there is a substantial difference in the extremes depending on the defini-
476 tion of yearly blocks used in the extreme value analysis (Figure 2). These
477 differences were most notable in the Southern hemisphere, and in locations
478 where the driest month occurs around June (Figure S1). Although there is
479 no systematic bias, we still recommend to apply the extreme value analyses
480 for estimating extreme precipitation based on hydrological years in future

481 studies. Our analysis indicates that this can be particularly relevant in the
482 Southern hemisphere and in regions characterized by marked seasonal cycles.

483 It is well known that the traditional GEV and POT methods require very
484 long data-series for accurate estimation of the tail behavior, and our study
485 confirms that there is a low spatial coherence for the tail properties of both
486 distributions (Figure 6a and b) using just 38 years of training data. The tail
487 properties of the MEV distribution are spatially more coherent (Figure 6c)
488 and hence the estimated return levels are more spatially coherent as well
489 (Figure 3c). This spatially coherent behavior, consistent with previous results
490 obtained over the conterminous US (Zorzetto and Marani, 2020), shows that
491 the MEV distribution is able to capture spatially consistent tail behavior
492 from short time series and by a single grid-cell analysis, without any prior
493 information on the spatial precipitation structures. The analysis of the MEV
494 tail behavior reveals distinct spatial patterns, as the heaviness appears to be
495 controlled by climate zones and orography. Heavier tails are observed in arid
496 areas, and thinner tails in mountainous regions. More in-depth analyses are
497 necessary to draw definite conclusions on what exactly controls the heaviness
498 of extreme value distribution tails. The performance of MEV is promising
499 for regions without long local precipitation records. Furthermore, our study
500 shows that the tail behavior captured by MEV is coherent and heavy both
501 spatially and temporally (Figures 6, 7 and S5-S11). For GEV and POT, on
502 the other hand, the tail behavior decreases with increased event duration,
503 resulting in a thin tail with a finite endpoint for about half of the cells for a
504 duration of 10 days.

505 We also conclude that both GEV and POT generally underestimate the
506 observed extremes, whereas MEV overestimates them (Figure 5). This occurs
507 particularly for long-duration extremes and large return periods. We do
508 consider it likely, however, that the results could be improved, for instance
509 by changing the event threshold or by fitting the Weibull distribution over
510 two or more years for dry areas (Miniussi and Marani, 2020), so as to reduce
511 inter-annual variability of the parameters due to samples of limited length.
512 Our results suggest that this issue is particularly relevant at the longest
513 durations examined. For GEV and POT the results could also be improved
514 by adopting spatial models (Davison et al., 2012; Huser and Wadsworth,
515 2020).

516 The data generated for this study are openly available as the GPEX
517 dataset (Gründemann et al., 2021). These data include extreme precipitation
518 return levels and extreme value distribution parameters for durations between

519 3 hours and 10 days at a global gridded 0.1° resolution. They could be used
520 by engineers as a reference of precipitation extremes for data-scarce regions
521 in particular. For scientific purposes, all underlying parameters are also
522 available and can be used to answer several outstanding questions, such as:
523 what are the controls on the tail behavior of extremes, and what is driving
524 the different changes in tail heaviness with duration for GEV, POT, and
525 MEV?.

526 **Declaration of Interest**

527 The authors declare that they have no known competing financial inter-
528 ests or personal relationships that could have appeared to influence the work
529 reported in this paper.

530 **Acknowledgments**

531 We acknowledge the use of the `mevpy` Python package (<https://github.com/EnricoZorretto/mevpy>) for the extreme value analysis. This work was
532 carried out on the Dutch National e-Infrastructure (DNI) with support from
533 the SURF cooperative. Enrico Zorretto acknowledges support from the
534 NASA Earth and Space Science Fellowship 80NSSC17K0364. Hylke Beck
535 was supported in part by the U.S. Army Corps of Engineers' International
536 Center for Integrated Water Resources Management (ICIWaRM). Nick van
537 de Giesen acknowledges support of the European Commission's Horizon 2020
538 Programme under grant agreement number 776691 (TWIGA). Ruud van der
539 Ent acknowledges funding from the Netherlands Organization for Scientific
540 Research (NWO), project number 016.Veni.181.015.

542 The GPEX dataset is available at the 4TU repository Gründemann et al.
543 (2021). The data included are the extremes estimated using the different
544 distributions, the observed extremes, and the parameters to estimate the ex-
545 tremes. These data are available for all durations included in this study. The
546 resolution of the dataset is 0.1° , the resolution of the MSWEP-V2.2 dataset.
547 For more information we refer to the Dataset Usage Notes in Section 5 of the
548 supplementary material.

549 **References**

550 Alijanian, M., Rakhshandehroo, G.R., Mishra, A.K., Dehghani, M., 2017.
551 Evaluation of satellite rainfall climatology using CMORPH, PERSIANN-

- 552 CDR, PERSIANN, TRMM, MSWEP over Iran. *International Journal of*
553 *Climatology* 37, 4896–4914. doi:10.1002/joc.5131.
- 554 Allan, R.P., Soden, B.J., 2008. Atmospheric warming and the amplification
555 of precipitation extremes. *Science* 321, 1481–1484. doi:10.1126/science.
556 1160787.
- 557 Arguez, A., Vose, R.S., 2011. The definition of the standard WMO cli-
558 mate normal: The key to deriving alternative climate normals. *Bul-*
559 *letin of the American Meteorological Society* 92, 699–704. doi:10.1175/
560 2010BAMS2955.1.
- 561 Bai, P., Liu, X., 2018. Evaluation of five satellite-based precipitation products
562 in two gauge-scarce basins on the Tibetan Plateau. *Remote Sensing* 10.
563 doi:10.3390/RS10081316.
- 564 Ball, J., Babister, M., Nathan, R., Weeks, W., Weinmann, E., Retallick,
565 M., Testoni, I., 2019. Australian Rainfall and Runoff: A guide to flood
566 estimation. Commonwealth of Australia (Geoscience Australia).
- 567 Beck, H.E., Pan, M., Roy, T., Weedon, G.P., Pappenberger, F., van
568 Dijk, A.I.J.M., Huffman, G.J., Adler, R.F., Wood, E.F., 2019a. Daily
569 evaluation of 26 precipitation datasets using Stage-IV gauge-radar data
570 for the CONUS. *Hydrology and Earth System Sciences* 23, 207–224.
571 doi:10.5194/hess-23-207-2019.
- 572 Beck, H.E., Vergopolan, N., Pan, M., Levizzani, V., van Dijk, A.I.M., Wee-
573 don, G.P., Brocca, L., Pappenberger, F., Huffman, G.J., Wood, E.F., 2017.
574 Global-scale evaluation of 22 precipitation datasets using gauge observa-
575 tions and hydrological modeling. *Hydrology and Earth System Sciences*
576 21, 6201–6217. doi:10.5194/hess-21-6201-2017.
- 577 Beck, H.E., Wood, E.F., Pan, M., Fisher, C.K., Miralles, D.G., van Dijk,
578 A.I.J.M., McVicar, T.R., Adler, R.F., 2019b. MSWEP V2 Global 3-
579 Hourly 0.1° Precipitation: Methodology and Quantitative Assessment.
580 *Bulletin of the American Meteorological Society* 100, 473–500. doi:10.
581 1175/BAMS-D-17-0138.1.
- 582 Becker, A., Finger, P., Meyer-Christoffer, A., Rudolf, B., Schamm, K.,
583 Schneider, U., Ziese, M., 2013. A description of the global land-surface

- 584 precipitation data products of the global precipitation climatology centre
585 with sample applications including centennial (trend) analysis from 1901-
586 present. *Earth System Science Data* 5, 71. doi:10.5194/essd-5-71-2013.
- 587 Beersma, J., Versteeg, R., Hakvoort, H., 2018. Neerslagstatistieken voor
588 korte duren actualisatie 2018. Technical Report. STOWA. Amersfoort.
- 589 Casson, D.R., Werner, M., Weerts, A., Solomatine, D., 2018. Global re-
590 analysis datasets to improve hydrological assessment and snow water equiv-
591 alent estimation in a sub-arctic watershed. *Hydrology and Earth System
592 Sciences* 22, 4685–4697. doi:10.5194/hess-22-4685-2018.
- 593 Cavanaugh, N.R., Gershunov, A., 2015. Probabilistic tail dependence
594 of intense precipitation on spatiotemporal scale in observations, reanal-
595 yses, and GCMs. *Climate Dynamics* 45, 2965–2975. doi:10.1007/
596 s00382-015-2517-1.
- 597 Cavanaugh, N.R., Gershunov, A., Panorska, A.K., Kozubowski, T.J., 2015.
598 The probability distribution of intense daily precipitation. *Geophysical
599 Research Letters* 42, 1560–1567. doi:10.1002/2015GL063238.
- 600 Coles, S., 2001. An introduction to statistical modeling of extreme values.
601 Springer Series in Statistics; Springer: London, UK.
- 602 Contractor, S., Donat, M., Alexandre, L.V., Ziese, M., Meyer-Christoffer,
603 A., Schneider, U., Rustemeier, E., Becker, A., Durre, I., Vose, R.S., 2020.
604 Rainfall estimates on a gridded network (regen)—a global land-based grid-
605 ded dataset of daily precipitation from 1950 to 2016. *Hydrology and Earth
606 System Sciences* 24, 919–943. doi:10.5194/hess-24-919-2020.
- 607 Courty, L.G., Wilby, R.L., Hillier, J.K., Slater, L.J., 2019. Intensity-duration-
608 frequency curves at the global scale. *Environmental Research Letters* 14,
609 084045. doi:10.1088/1748-9326/ab370a.
- 610 CRED, 2019. Natural disasters 2018. Technical Report. Institute Health
611 and Society UClouvain. Brussels, Belgium. URL: [https://www.cred.be/
612 sites/default/files/CREDNaturalDisaster2018.pdf](https://www.cred.be/sites/default/files/CREDNaturalDisaster2018.pdf).
- 613 Davison, A.C., Padoan, S.A., Ribatet, M., et al., 2012. Statistical modeling
614 of spatial extremes. *Statistical science* 27, 161–186.

- 615 Davison, A.C., Smith, R.L., 1990. Models for Exceedances over High Thresh-
616 olds. *Journal of the Royal Statistical Society. Series B (Methodological)*
617 52, 393–442. URL: <https://www.jstor.org/stable/2345667>.
- 618 De Paola, F., Giugni, M., Pugliese, M., Annis, A., Nardi, F., 2018.
619 GEV parameter estimation and stationary vs. non-stationary analysis
620 of extreme rainfall in African test cities. *Hydrology* 5. doi:10.3390/
621 hydrology5020028.
- 622 Decker, M., Brunke, M.A., Wang, Z., Sakaguchi, K., Zeng, X., Bosilovich,
623 M.G., 2012. Evaluation of the Reanalysis Products from GSFC, NCEP,
624 and ECMWF Using Flux Tower Observations. *Journal of Climate* 25,
625 1916–1944. doi:10.1175/JCLI-D-11-00004.1.
- 626 Demirdjian, L., Zhou, Y., Huffman, G.J., 2018. Statistical modeling of ex-
627 treme precipitation with trmm data. *Journal of applied meteorology and*
628 *climatology* 57, 15–30. doi:10.1175/JAMC-D-17-0023.1.
- 629 Donat, M.G., Alexander, L.V., Yang, H., Durre, I., Vose, R., Dunn, R.J.,
630 Willett, K.M., Aguilar, E., Brunet, M., Caesar, J., Hewitson, B., Jack,
631 C., Klein Tank, A.M., Kruger, A.C., Marengo, J., Peterson, T.C., Renom,
632 M., Oria Rojas, C., Rusticucci, M., Salinger, J., Elrayah, A.S., Sekele, S.S.,
633 Srivastava, A.K., Trewin, B., Villarroel, C., Vincent, L.A., Zhai, P., Zhang,
634 X., Kitching, S., 2013. Updated analyses of temperature and precipitation
635 extreme indices since the beginning of the twentieth century: The HadEX2
636 dataset. *Journal of Geophysical Research: Atmospheres* 118, 2098–2118.
637 doi:10.1002/jgrd.50150.
- 638 Gelaro, R., McCarty, W., Suárez, M.J., Todling, R., Molod, A., Takacs, L.,
639 Randles, C.A., Darmenov, A., Bosilovich, M.G., Reichle, R., Wargan, K.,
640 Coy, L., Cullather, R., Draper, C., Akella, S., Buchard, V., Conaty, A.,
641 Da Silva, A.M., Wei, G., Kim, G.K., Koster, R., Lucchesi, R., Merkova,
642 D., Nielsen, J.E., Partyka, G., Pawson, S., Putman, W., Rienecker, M.,
643 Schubert, S.D., Sienkiewicz, M., Zhao, B., 2017. The modern-era retro-
644 spective analysis for research and applications, version 2 (merra-2). *Journal*
645 *of Climate* 30, 5419–5454. doi:10.1175/JCLI-D-16-0758.1.
- 646 van de Giesen, N., Hut, R., Selker, J., 2014. The Trans-African Observatory
647 (TAHMO). *WIREs Water* 1, 341–348. doi:10.1002/wat2.1034.

- 648 Greenwood, J.A., Landwehr, J., Matalas, N., Wallis, J., 1979. Probabil-
649 ity weighted moments: definition and relation to parameters of several
650 distributions expressible in inverse form. *Water Resources Research* 15,
651 1049–1054. doi:10.1029/WR015i005p01049.
- 652 Gründemann, G.J., Werner, M., Veldkamp, T.I.E., 2018. The poten-
653 tial of global reanalysis datasets in identifying flood events in southern
654 africa. *Hydrology and Earth System Sciences* 22, 4667–4683. doi:10.5194/
655 hess-22-4667-2018.
- 656 Gründemann, G.J., Zorzetto, E., Beck, H.E., Schleiss, M., van de Giesen,
657 N., Marani, M., van der Ent, R.J., 2021. Global Precipitation EXtremes
658 dataset. doi:10.4121/uuid:12b5c941-cd54-45db-8d7b-efaaacecaa69.
- 659 Hersbach, H., Bell, B., Berrisford, P., Hirahara, S., Horanyi, A., Munoz-
660 Sabater, J., Nicolas, J., Peubey, C., Radu, R., Schepers, D., Simmons,
661 A., Soci, C., Abdalla, S., Abellan, X., Balsamo, G., Bechtold, P., Bia-
662 vati, G., Bidlot, J., Bonavita, M., Chiara, G.D., Dahlgren, P., Dee, D.,
663 Diamantakis, M., Dragani, R., Flemming, J., Forbes, R., Fuentes, M.,
664 Geer, A., Haimberger, L., Healy, S., Hogan, R.J., Holm, E., Janiskova, M.,
665 Keeley, S., Laloyaux, P., Lopez, P., Radnoti, G., de Rosnay, P., Rozum,
666 I., Vamborg, F., Villaume, S., Thepaut, J.N., 2020. The ERA5 global
667 reanalysis. *Quarterly Journal of the Royal Meteorological Society* , 1–
668 51doi:10.1002/qj.3803.
- 669 Hong, Y., Hsu, K.L., Sorooshian, S., Gao, X., 2004. Precipitation esti-
670 mation from remotely sensed imagery using an artificial neural network
671 cloud classification system. *Journal of Applied Meteorology* 43, 1834–1853.
672 doi:10.1175/JAM2173.1.
- 673 Hosking, J.R.M., 1990. L-Moments: Analysis and estimation of distribu-
674 tions using linear combinations of order statistics. *Journal of the Royal*
675 *Statistical Society. Series B (Methodological)* 52, 105–124.
- 676 Hosking, J.R.M., Wallis, J.R., 1987. Parameter and Quantile Estimation for
677 the Generalized Pareto Distribution Parameter and Quantile Estimation
678 Generalized Pareto Distribution. *Technometrics* 23, 339–349. doi:https:
679 //doi.org/10.1080/00401706.1987.10488243.

- 680 Hosseini, S.R., Scaioni, M., Marani, M., 2020. Extreme Atlantic Hur-
681 ricane Probability of Occurrence Through the Metastatistical Extreme
682 Value Distribution. *Geophysical Research Letters* 47, 1–9. doi:10.1029/
683 2019GL086138.
- 684 Hu, L., Nikolopoulos, E.I., Marra, F., Morin, E., Marani, M., Anagnostou,
685 E.N., 2020. Evaluation of MEVD-based precipitation frequency analyses
686 from quasi- global precipitation datasets against dense rain gauge net-
687 works. *Journal of Hydrology* 590, 125564. doi:10.1016/j.jhydrol.2020.
688 125564.
- 689 Huffman, G.J., Bolvin, D.T., Braithwaite, D., Hsu, K., Joyce, R., Kidd,
690 C., Nelkin, E.J., Xie, P., 2015. NASA Global Precipitation Measurement
691 (GPM) Integrated Multi-satellitE Retrievals for GPM (IMERG): Algo-
692 rithm Theoretical Basis Document (ATBD) Version 4.5. Technical Report.
693 NASA/GSFC, Greenbelt, MD 20771, USA.
- 694 Huser, R., Wadsworth, J.L., 2020. Advances in statistical modeling of spatial
695 extremes. *Wiley Interdisciplinary Reviews: Computational Statistics* ,
696 e1537.
- 697 Joyce, R.J., Janowiak, J.E., Arkin, P.A., Xie, P., 2004. CMORPH: A method
698 that produces global precipitation estimates from passive microwave and
699 infrared data at high spatial and temporal resolution. *Journal of Hydrom-
700 eteorology* 5, 487–503.
- 701 Kendon, E.J., Blenkinsop, S., Fowler, H.J., 2018. When will we detect
702 changes in short-duration precipitation extremes? *Journal of Climate*
703 31, 2945–2964. doi:10.1175/JCLI-D-17-0435.1.
- 704 Kidd, C., Becker, A., Huffman, G.J., Muller, C.L., Joe, P., Skofronick-
705 Jackson, G., Kirschbaum, D.B., 2017. So, how much of the Earth’s surface
706 is covered by rain gauges? *Bulletin of the American Meteorological Society*
707 98, 69–78. doi:10.1175/BAMS-D-14-00283.1.
- 708 Kobayashi, S., Ota, Y., Harada, Y., Ebata, A., Moriya, M., Onoda, H.,
709 Onogi, K., Kamahori, H., Kobayashi, C., Endo, H., et al., 2015. The jra-55
710 reanalysis: General specifications and basic characteristics. *Journal of the
711 Meteorological Society of Japan* 93, 5–48. doi:10.2151/jmsj.2015-001.

- 712 Koutsoyiannis, D., 2004a. Statistics of extremes and estimation of extreme
713 rainfall: I. Theoretical investigation. *Hydrological Sciences Journal* 49,
714 575–590. doi:10.1623/hysj.49.4.575.54430.
- 715 Koutsoyiannis, D., 2004b. Statistics of extremes and estimation of extreme
716 rainfall: II. Empirical investigation of long rainfall records. *Hydrological
717 Sciences Journal* 49, 591–610. doi:10.1623/hysj.49.4.591.54424.
- 718 Laherrere, J., Sornette, D., 1998. Stretched exponential distributions in
719 nature and economy: “fat tails” with characteristic scales. *The European
720 Physical Journal B-Condensed Matter and Complex Systems* 2, 525–539.
- 721 Liu, Z., Liu, Y., Wang, S., Yang, X., Wang, L., Baig, M.H.A., Chi, W.,
722 Wang, Z., 2018. Evaluation of Spatial and Temporal Performances of
723 ERA-Interim Precipitation and Temperature in Mainland China. *Journal
724 of Climate* 31, 4347–4365. doi:10.1175/JCLI-D-17-0212.1.
- 725 Mailhot, A., Duchesne, S., 2009. Design criteria of urban drainage infras-
726 tructures under climate change. *Journal of Water Resources Planning and
727 Management* 136, 201–208. doi:10.1061/(asce)wr.1943-5452.0000023.
- 728 Marani, M., Ignaccolo, M., 2015. A metastatistical approach to rainfall
729 extremes. *Advances in Water Resources* 79, 121–126. doi:10.1016/j.
730 advwatres.2015.03.001.
- 731 Marani, M., Zanetti, S., 2015. Long-term oscillations in rainfall extremes
732 in a 268 year daily time series. *Water Resources Research* 51, 639–647.
733 doi:10.1002/2014WR015885.
- 734 Marra, F., Borga, M., Morin, E., 2020. A unified framework for extreme
735 subdaily precipitation frequency analyses based on ordinary events. *Geo-
736 physical Research Letters* 47, e2020GL090209.
- 737 Marra, F., Nikolopoulos, E.I., Anagnostou, E.N., Bárdossy, A., Morin, E.,
738 2019a. Precipitation frequency analysis from remotely sensed datasets: A
739 focused review. *Journal of Hydrology* 574, 699–705.
- 740 Marra, F., Nikolopoulos, E.I., Anagnostou, E.N., Morin, E., 2018. Metas-
741 tatistical Extreme Value analysis of hourly rainfall from short records:
742 Estimation of high quantiles and impact of measurement errors. *Advances
743 in Water Resources* 117, 27–39. doi:10.1016/j.advwatres.2018.05.001.

- 744 Marra, F., Zoccatelli, D., Armon, M., Morin, E., 2019b. A simplified
745 MEV formulation to model extremes emerging from multiple nonstation-
746 ary underlying processes. *Advances in Water Resources* 127, 280–290.
747 doi:10.1016/j.advwatres.2019.04.002.
- 748 McGraw, D., Nikolopoulos, E.I., Marra, F., Anagnostou, E.N., 2019. Pre-
749 cipitation frequency analyses based on radar estimates: An evaluation
750 over the contiguous United States. *Journal of Hydrology* 573, 299–310.
751 doi:10.1016/j.jhydrol.2019.03.032.
- 752 Ménégoz, M., Gallée, H., Jacobi, H.W., 2013. Precipitation and snow
753 cover in the himalaya: from reanalysis to regional climate simulations.
754 *Hydrology and Earth System Sciences* 17, 3921–3936. doi:10.5194/
755 hess-17-3921-2013.
- 756 Miniussi, A., Marani, M., 2020. Estimation of daily rainfall extremes through
757 the metastatistical extreme value distribution: Uncertainty minimiza-
758 tion and implications for trend detection. *Water Resources Research* 56,
759 e2019WR026535. doi:10.1029/2019WR026535.
- 760 Miniussi, A., Marani, M., Villarini, G., 2020a. Metastatistical Extreme Value
761 Distribution applied to floods across the continental United States. *Ad-
762 vances in Water Resources* 136, 103498. doi:10.1016/j.advwatres.2019.
763 103498.
- 764 Miniussi, A., Villarini, G., Marani, M., 2020b. Analyses Through the Metas-
765 tatistical Extreme Value Distribution Identify Contributions of Tropical
766 Cyclones to Rainfall Extremes in the Eastern United States *Geophys-
767 ical Research Letters*. *Geophysical Research Letters* 47, e2020GL087238.
768 doi:10.1029/2020GL087238.
- 769 Mishra, A.K., Coulibaly, P., 2009. Developments in hydrometric network
770 design: A review. *Reviews of Geophysics* 47. doi:10.1029/2007RG000243.
- 771 Nissen, K.M., Ulbrich, U., 2017. Increasing frequencies and changing charac-
772 teristics of heavy precipitation events threatening infrastructure in Europe
773 under climate change. *Natural Hazards and Earth System Sciences* 17,
774 1177–1190. doi:10.5194/nhess-17-1177-2017.

- 775 Overeem, A., Buishand, A., Holleman, I., 2008. Rainfall depth-duration-
776 frequency curves and their uncertainties. *Journal of Hydrology* 348, 124–
777 134. doi:10.1016/j.jhydro1.2007.09.044.
- 778 Papalexiou, S.M., Aghakouchak, A., Foufoula-Georgiou, E., 2018. A diagnos-
779 tic framework for understanding climatology of tails of hourly precipitation
780 extremes in the United States. *Water Resources Research* 54, 6725–6738.
781 doi:10.1029/2018WR022732.
- 782 Papalexiou, S.M., Koutsoyiannis, D., 2013. Battle of extreme value distribu-
783 tions: A global survey on extreme daily rainfall. *Water Resources Research*
784 49, 187–201. doi:10.1029/2012WR012557.
- 785 Papalexiou, S.M., Koutsoyiannis, D., Makropoulos, C., 2013. How extreme
786 is extreme? An assessment of daily rainfall distribution tails. *Hydrology
787 and Earth System Sciences* 17, 851–862. doi:10.5194/hess-17-851-2013.
- 788 Perica, S., Pavlovic, S., St. Laurent, M., Trypaluk, C., Unruh, D., Martin,
789 D., Wilhite, O., 2015. NOAA Atlas 14 Volume 10, Precipitation-Frequency
790 Atlas of the United States, Northeastern States. Technical Report. NOAA,
791 National Weather Service.
- 792 Perica, S., Pavlovic, S., St. Laurent, M., Trypaluk, C., Unruh, D., Wilhite,
793 O., 2018. NOAA Atlas 14: Precipitation-frequency atlas of the United
794 States, Texas. Technical Report. NOAA, National Weather Service.
- 795 Ragulina, G., Reitan, T., 2017. Generalized extreme value shape parameter
796 and its nature for extreme precipitation using long time series and the
797 Bayesian approach precipitation. *Hydrological Sciences Journal* 62, 863–
798 879. doi:10.1080/02626667.2016.1260134.
- 799 Rasmusson, E.M., Arkin, P.A., 1993. A global view of large-scale precipita-
800 tion variability. *Journal of Climate* 6, 1495–1522.
- 801 Sahlu, D., Moges, S.A., Nikolopoulos, E.I., Anagnostou, E.N., Hailu, D.,
802 2017. Evaluation of high-resolution multisatellite and reanalysis rainfall
803 products over East Africa. *Advances in Meteorology* 2017. doi:10.1155/
804 2017/4957960.
- 805 Satgé, F., Ruelland, D., Bonnet, M.P., Molina, J., Pillco, R., 2019. Con-
806 sistency of satellite-based precipitation products in space and over time

- 807 compared with gauge observations and snow-hydrological modelling in the
808 Lake Titicaca region. *Hydrology and Earth System Sciences* 23, 595–619.
809 doi:10.5194/hess-23-595-2019.
- 810 Schellander, H., Lieb, A., Hell, T., 2019. Error structure of metastatistical
811 and generalized extreme value distributions for modeling extreme rainfall
812 in austria. *Earth and Space Science* 6, 1616–1632.
- 813 Schneider, U., Becker, A., Finger, P., Meyer-Christoffer, A., Rudolf, B., Ziese,
814 M., 2011. GPCP full data reanalysis version 6.0 at 0.5°: Monthly land-
815 surface precipitation from rain-gauges built on GTS-based and historic
816 data. doi:10.5676/DWD_GPCP/FD_M_V6_050.
- 817 Schneider, U., Becker, A., Finger, P., Meyer-Christoffer, A., Ziese, M.,
818 Rudolf, B., 2014. GPCP’s new land surface precipitation climatology
819 based on quality-controlled in situ data and its role in quantifying the
820 global water cycle. *Theoretical and Applied Climatology* 115, 15–40.
821 doi:10.1007/s00704-013-0860-x.
- 822 Serinaldi, F., Kilsby, C.G., 2014. Rainfall extremes: Toward reconciliation
823 after the battle of distributions. *Water Resources Research* 50, 336–352.
824 doi:10.1002/2013WR014211.
- 825 Sun, Q., Miao, C., Duan, Q., Ashouri, H., Sorooshian, S., Hsu, K., 2018.
826 A review of global precipitation data sets: Data sources, estimation,
827 and intercomparisons. *Review of Geophysics* 56, 79–107. doi:10.1002/
828 2017RG000574.
- 829 UNSIDR, 2015. Sendai Framework for Disaster Risk Reduction 2015 - 2030.
830 Technical Report. URL: [www.unisdr.org/we/inform/publications/
831 43291](http://www.unisdr.org/we/inform/publications/43291).
- 832 Ushio, T., Sasashige, K., Kubota, T., Shige, S., Okamoto, K., Aonashi, K.,
833 Inoue, T., Takahashi, N., Iguchi, T., Kachi, M., Oki, R., Morimoto, T.,
834 Kawasaki, Z.I., 2009. A kalman filter approach to the Global Satellite
835 Mapping of Precipitation (GSMaP) from combined passive microwave and
836 infrared radiometric data. *Journal of the Meteorological Society of Japan*
837 87 A, 137–151. doi:10.2151/jmsj.87A.137.
- 838 Villarini, G., Smith, J.A., Lynn, M., Vitolo, R., Stephenson, D.B., Krajewski,
839 W.F., 2011. On the frequency of heavy rainfall for the Midwest of

- 840 the United States. *Journal of Hydrology* 400, 103–120. doi:10.1016/j.
841 jhydrol.2011.01.027.
- 842 Ward, P.J., Kummu, M., Lall, U., 2016. Flood frequencies and durations and
843 their response to El Niño Southern Oscillation: Global analysis. *Journal*
844 *of Hydrology* 539, 358–378. doi:10.1016/j.jhydrol.2016.05.045.
- 845 Wasko, C., Sharma, A., Johnson, F., 2015. Does storm duration modulate
846 the extreme precipitation-temperature scaling relationship? *Geophysical*
847 *Research Letters* 42, 8783–8790. doi:10.1002/2015GL066274.
- 848 Westra, S., Alexander, L.V., Zwiers, F.W., 2013. Global increasing trends in
849 annual maximum daily precipitation. *Journal of Climate* 26, 3904–3918.
850 doi:10.1175/JCLI-D-12-00502.1.
- 851 Wilson, P.S., Toumi, R., 2005. A fundamental probability distribution
852 for heavy rainfall. *Geophysical Research Letters* 32. doi:10.1029/
853 2005GL022465.
- 854 Zhang, D., Liu, X., Bai, P., Li, X.H., 2019. Suitability of satellite-based pre-
855 cipitation products for water balance simulations using multiple observa-
856 tions in a humid catchment. *Remote Sensing* 11. doi:10.3390/rs11020151.
- 857 Zorzetto, E., Botter, G., Marani, M., 2016. On the emergence of rainfall
858 extremes from ordinary events. *Geophysical Research Letters* 43, 8076–
859 8082. doi:10.1002/2016GL069445.
- 860 Zorzetto, E., Marani, M., 2019. Downscaling of rainfall extremes from satel-
861 lite observations. *Water Resources Research* 55, 156–174. doi:10.1029/
862 2018WR022950.
- 863 Zorzetto, E., Marani, M., 2020. Extreme value metastatistical analysis of
864 remotely sensed rainfall in ungauged areas: Spatial downscaling and error
865 modelling. *Advances in Water Resources* 135, 103483. doi:10.1016/j.
866 advwatres.2019.103483.